

AD-A172 132

MROSS (NAVY REMOTE OCEAN SENSING SYSTEM) TRACKING  
NETWORK ANALYSIS(U) TEXAS UNIV AT AUSTIN CENTER FOR  
SPACE RESEARCH B D TAPLEY ET AL. 1986 N00014-85-K-2034

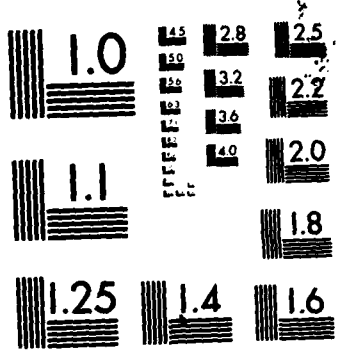
1/1

UNCLASSIFIED

F/G 4/2

NL





MICROCOPY RESOLUTION TEST CHART  
NATIONAL BUREAU OF STANDARDS-1963-A

12

AD-A172 132

### NROSS TRACKING NETWORK ANALYSIS

B. D. Tapley, J. C. Ries and C. Rajasenan  
Center for Space Research  
The University of Texas at Austin  
Austin, Texas 78712

DTIC  
SELECTE  
SEP 22 1986  
S  
D

#### 1. INTRODUCTION

The Navy Remote Ocean Sensing System (NROSS) mission is designed to coincide with the TOPEX mission. One of the main objectives of the mission is the daily production of mesoscale feature maps of selected ocean areas. The NROSS payload will include a SEASAT-class altimeter for the production of these maps and a scatterometer to measure wind speed and direction over the oceans. In addition to meeting a number of the U.S. Navy's fleet operation requirements, these wind measurements will be used in conjunction with the precision altimetry from TOPEX to examine the relationship between ocean circulation and winds. → (to p 13)

The NROSS payload will also include a TRANET beacon comparable to the one currently orbiting on GEOSAT, which will be used to satisfy the orbit determination requirements for NROSS. The radial orbit accuracy achievable with such a tracking system will depend on the ground-based satellite doppler tracking network employed for the mission. Both the number of stations and the accuracy with which their coordinates are known will be factors in the ephemeris accuracy. This study evaluates the effect on the radial orbit accuracy of three possible tracking station deployment scenarios for the NROSS mission. The three scenarios are:

- A. the complete TRANET network plus the OPNET network,
- B. the permanent sites of the TRANET network and
- C. the OPNET network.

The effect of the dominant error sources in the force and measurement models is evaluated for each of the tracking options.

DISTRIBUTION STATEMENT A  
Approved for public release;  
Distribution Unlimited

DTIC FILE COPY

06 8 6 025

## 2. DOPPLER MEASUREMENT

The doppler measurement is the integral of the cycles of a beat frequency ( $f_g - f_r$ ) which results from mixing the ground based reference frequency  $f_g$  and the frequency of the received satellite signal  $f_r$ . The basic measurement is the integrated count  $D$  between reception times  $\tau_1$  and  $\tau_2$  and is given by:

$$D = \int_{\tau_1}^{\tau_2} (f_g - f_r) d\tau \quad (1)$$

The number of cycles of the received frequency  $f_r$  between reception times  $\tau_1$  and  $\tau_2$  is equal to the number of cycles of the satellite transmission frequency  $f_s$  emitted between satellite time marks  $t_1$  and  $t_2$ , i.e

$$\int_{\tau_1}^{\tau_2} f_r d\tau = \int_{t_1}^{t_2} f_s dt \quad (2)$$

If  $f_g$  and  $f_s$  are assumed constant during the count interval, then Eq. (1) becomes:

$$D = f_g(\tau_2 - \tau_1) - f_s(t_2 - t_1) \quad (3)$$

Define  $t_1 = \tau_1 - \frac{s_1}{c}$  and  $t_2 = \tau_2 - \frac{s_2}{c}$  where  $s_i$  are the scalar ranges to the satellite from the ground station and are given by:

$$s_i = \left| \mathbf{r}_s(t_i) - \mathbf{r}_g(\tau_i) \right| \quad (4)$$

$\mathbf{r}_s(t_i)$  is the satellite position vector at time  $t_i$  and  $\mathbf{r}_g(\tau_i)$  is the ground station position vector at time  $\tau_i$ . Eq. (3) can now be written as:

$$D = (f_g - f_s)(\tau_2 - \tau_1) + \frac{f_s}{c}(s_2 - s_1)$$



*ltr. on file*  
(5)

Reliability Codes

Dist	Avail and/or Special
A-1	

The doppler count measurement can be preprocessed into average range-rate observations by rearranging Eq. (5) into:

$$\frac{s_2 - s_1}{\tau_2 - \tau_1} = \frac{c}{f_s(\tau_2 - \tau_1)} D + c \left\{ 1 - \frac{f_g}{f_s} \right\} \quad (6)$$

Eq. (6) is the average range-rate model used in this study. If the oscillator is sufficiently stable over the time span of the pass then receiver oscillator error introduces a constant bias into the average range-rate observation. The times  $\tau_1$  and  $\tau_2$  bound the individual measurements which for this study was assumed to be a 30-second interval.

The many different receivers used in the TRANET and OPNET networks and the fact that receiver frequency error simply biases the observations are the reasons for always determining the individual pass biases as a part of the orbit determination process. The oscillator frequency error is a "commission" error in the measurement process as distinct from the errors due to the media effects such as troposphere and ionosphere effects. The errors due to the media correction are due to deficiencies in our physical models for these effects. To mitigate the effects of refraction modeling errors, doppler data below 10° elevations was not used.

To correct for the effects of the ionospheric refraction, signals are transmitted at two different frequencies. The two frequencies are combined to eliminate nearly all of the effects of the ionosphere. The residual errors remaining after the two-frequency correction are generally small but not necessarily insignificant.

### 3. SIMULATION MODEL

Simulated average range-rate observations were generated for each tracking station location in the complete TRANET and OPNET networks using a "true" orbit with an epoch of 0<sup>h</sup>0<sup>m</sup>0.0<sup>s</sup>, 21 July 1978 and the following initial conditions:

- Semi-major axis  $a = 7211145$  meters
- Eccentricity  $e = 0.001$
- Inclination  $i = 98.739^\circ$
- Argument of ascending node  $\Omega = 0^\circ$
- Argument of perigee  $\omega = 45^\circ$
- Mean anomaly  $M = 0^\circ$

NROSS is scheduled to be launched in 1990 into a sun-synchronous orbit [1], when solar activity will reach the maximum value of its eleven-year cycle. The above epoch corresponds to a maximum solar activity period and should simulate the atmospheric density conditions to be encountered by NROSS.

The dynamic model used to generate the "true" orbit includes the following force effects:

- Gravity (GEM-10B complete to degree and order 36)
- Drag (constant satellite area, Jacchia-Roberts (1971) density model)
- Solar radiation pressure (constant satellite area, conical earth shadow model)
- Luni-solar perturbations (JPL DE-96 ephemeris)
- Solid earth tides

The assumptions of constant area models for drag and solar radiation pressure were made in the absence of a detailed description of the satellite configuration which was modeled as:

- Satellite mass = 1400 kg
- Surface area of satellite = 22 m<sup>2</sup>
- Coefficient of drag = 3.0
- Solar radiation pressure reflectivity coefficient = 0.27

Average range-rate measurements were generated with a 30-second count interval and an elevation cut-off angle of 10 degrees at each of the 43 stations listed in Table 1. A random

**TABLE 1**  
**STATION CORDINATES FOR THE**  
**TRANET AND OPNET STATIONS**

No	Station location	Longitude (deg)	Latitude (deg)
1	Smithfield (Australia)	138.654	-34.673
2	Barton Stacey (UK)	358.618	51.184
3	Brussels (Belgium)	4.358	50.798
4	Mizusawa (Japan)	141.133	39.135
5	Wetzell (FRG)	12.877	49.145
6	Herndon (USA)	282.686	38.995
7	Las Cruces (USA)	253.246	32.278
8	Guam (USA)	144.634	13.439
9	Pretoria (South Africa)	28.347	-25.946
10	San Jose (Brazil)	314.130	-23.217
11	Anchorage (USA)	210.174	61.283
12	Thule (Greenland)	291.245	76.535
13	Mahe (Seychelles)	55.479	-4.670
14	San Miguel (Philippines)	120.072	14.987
15	Tafuna (Samoa)	189.284	-14.329
16	Austin (USA)	262.274	30.383
17	McMurdo (Antartica)	166.673	-77.847
18	Calgary (Canada)	245.706	50.871
19	Ottawa (Canada)	284.081	45.399
20	Kiruna (Sweden)	20.216	67.825
21	Ouagadougou (Upper Volta)	358.503	12.403
22	Kerguelen	70.255	-49.352
23	Tahiti	210.416	-17.583
24	Ascension Island (UK)	345.597	-7.907
25	Catania (Italy)	14.937	37.405
26	Quito (Ecuador)	281.579	-0.097
27	Kinshasa (Zaire)	15.307	-4.301
28	Cyprus	33.730	35.001
29	Hawaii (USA)	202.001	21.314
30	Santiago (Chile)	289.147	-33.624
31	Bangkok (Thailand)	100.594	13.792
32	Diego Garcia	72.376	-7.263
33	Cambridge Bay (Canada)	254.878	69.117
34	Bahrain	50.608	26.209
35	Asuncion (Paraguay)	302.386	-25.300
36	Ukiah (USA)	236.787	39.137
37	Shemya (USA)	174.103	52.728
38	Napier (New Zealand)	176.850	-39.466
39	Perth (Australia)	115.933	-31.600
40	OPNET1	291.987	44.212
41	OPNET2	240.935	33.929
42	OPNET3	202.004	21.391
43	OPNET4	266.920	44.538

measurement noise with a standard deviation of 1 mm/sec was added to the measurements. The doppler data distribution for a two-day arc in bins of 1 revolution is given in Figure 1. The geographical distribution of the tracking stations together with the visibility masks and the ground-track coverage are illustrated in Figure 2.

#### 4. ERROR MODELS

The analysis was based on a simulated doppler data set and hence error models were generated to study the effects of force and measurement model errors on the radial orbit accuracy. The orbit errors were simulated by generating a "nominal" orbit with a different force and/or measurement model to that used to generate the "true" orbit. The various force error models used were:

- Gravity (G10M50)
  - $G10M50 = GEM10B - 0.5*(GEM10B - GEML2)$
- Drag (Asymmetric modified Harris-Priester density model)
- Solar radiation pressure (10 percent error in  $\eta$ )

The gravity error model was developed by differencing the spherical harmonic coefficients of two different geopotential models as described above. The GEML2 gravity model has coefficients defined to degree and order 20 [2] and the GEM10B model is complete to degree and order 36 [3]. Thus in the generation of the G10M50 model, in the cases where the GEM10B and GEML2 models did not have coefficients of common degree and order, the GEM10B coefficients were modified by 50 percent. Consequently the power of the error in the G10M50 model is weighted more towards the higher degree and order terms.

The error in the drag model was obtained by using two different atmospheric density models in the computation of the acceleration due to drag. The Jacchia-Roberts density model uses a static temperature profile whereas the asymmetric modified Harris-Priester density model uses a dynamic

temperature profile [4]. These differing approaches cause a systematic difference in the density profiles generated by the two models. The maximum difference in density determined by the two models is of the order of 15 percent.

Since the solar radiation pressure model adopted a constant area model, the error model was simulated by scaling the reflectivity coefficient  $\eta$  by 10 percent.

The measurement model errors included the effects of station coordinate errors and troposphere refraction errors. Station coordinate errors were simulated by modifying the earth-fixed station cartesian coordinates  $x$ ,  $y$  and  $z$  by 1 meter in a random fashion. The troposphere refraction errors were simulated in a random manner indirectly by introducing errors in the ambient values of relative humidity, temperature and pressure of magnitudes of 10 percent, 5 percent and 5 percent, respectively. To offset ignoring residual ionosphere refraction errors, the troposphere errors were chosen to be somewhat pessimistic.

## 5. ANALYSIS

The three tracking scenarios were evaluated for various error models. The analysis consisted of fitting a "nominal" orbit to the simulated doppler data by simultaneously estimating the satellite position and velocity at epoch  $(r_0, v_0)$ , the coefficient of drag ( $C_d$ ), the solar radiation pressure reflectivity coefficient ( $\eta$ ) and a measurement pass bias. The reflectivity coefficient  $\eta$  was not estimated when the solar radiation pressure model error was included. The fitted orbit was then compared to the "true" orbit and the root mean square (rms) values of the radial orbit differences were computed.

A basic problem in using doppler measurements is the large volume of data produced in comparison with other measurement types. In TRANET doppler practice, "short arc" orbit computations refers to data spans of 2 orbit revolutions and "long arc" refer to data spans of 2 days.

In the current study, 2-rev and 2-day arcs were used for the orbit comparisons.

### 5.1 Short arc analysis

The results of the short arc analysis for the various error models are shown in Table 2. The gravity model error is the predominant source of the radial orbit error. The effect of the gravity error on the radial orbit accuracy is an order of magnitude greater than the effects due to the drag and solar radiation pressure model errors. The effects of the troposphere refraction errors are greater than those due to the station coordinate errors. The radial orbit errors associated with Scenario C are much larger than those of Scenarios A and B because the data set for the particular 2-rev arc in Scenario C is much smaller than those of Scenarios A and B.

TABLE 2 NROSS DOPPLER TRACKING ANALYSIS 2-rev arc Root mean square radial orbit error (cm)				
Error Model	Estimate Parameters	Scenario A (43 stations)	Scenario B (23 stations)	Scenario C (4 stations)
1) Gravity model error (G10M50)	$r_0, v_0, C_d, \eta,$ pass biases	51	50	303
2) Drag model error (H.P vs J71)	"	2	2	321
3) S.r.p model error (10% in $\eta$ )	$r_0, v_0, C_d,$ pass biases	1.9	1.6	242
4) Station coordinate errors	$r_0, v_0, C_d, \eta$ pass biases	16	32	443
5) Troposphere refraction errors	"	25	42	5770
Number of observations		648	396	53
Number of pass biases		41	25	3

### 5.2 Long arc analysis

The results of the long arc analysis are summarized in Table 3. The effects of all force model errors have increased with the longer arc in Scenarios A and B, and the effects of all measurement

model errors have concurrently decreased. In Scenario C, the effects of both force and measurement model errors have decreased. This is due to the fact that the limited geographical distribution of tracking sites in Scenario C created a sparse data set for the 2-rev arc which was inadequate to provide a good orbit fit, whereas the longer arc created a fuller data set with better geographical distribution and provided a better orbit fit. That is, the reduction in radial orbit errors in Scenario C is due to a better distributed data set rather than due to the sensitivity to the various error models. The radial orbit accuracies achieved with Scenarios A and B are almost comparable.

TABLE 3 NROSS DOPPLER TRACKING ANALYSIS 2-day arc Root mean square radial orbit error (cm)				
Error Model	Estimate Parameters	Scenario A (43 stations)	Scenario B (23 stations)	Scenario C (4 stations)
1) Gravity model error (G10M50)	$r_0, v_0, C_d, \eta$ , pass biases	91	91	97
2) Drag model error (H.P vs J71)	"	12	12	13
3) S.r.p model error (10% in $\eta$ )	$r_0, v_0, C_d$ , pass biases	4.5	4.5	4.6
4) Station coordinate errors	$r_0, v_0, C_d, \eta$ , pass biases	7	9	13
5) Troposphere refraction errors	"	7	5	21
Number of observations		6774	3999	545
Number of pass biases		414	244	33

Table 4 lists radial orbit accuracies for different combinations of the various error models considered in the long arc analysis. Case 1 considers the effect of all force model errors including those due to gravity, drag and solar radiation pressure model errors acting together. The error model in Case 2 consists of all force model errors in Case 1 together with the station coordinate and troposphere refraction model errors. The inclusion of measurement model errors does not appreciably alter the performance of tracking Scenarios A and B. However the corresponding radial

orbit error computed in Scenario C increases by about 4 cm indicating its sensitivity to station coordinate and troposphere refraction errors. Case 3 lists the performance of the three tracking scenarios in the absence of gravity error. These values indicate the residual radial orbit error if it was possible to remove all gravity model errors by "tuning" the geopotential coefficients.

TABLE 4 NROSS DOPPLER TRACKING ANALYSIS 2-day arc Root mean square radial orbit error (cm)				
Error Model	Estimate Parameters	Scenario A (43 stations)	Scenario B (23 stations)	Scenario C (4 stations)
1) Gravity, drag and s.r.p errors	$r_0, v_0, C_d,$ pass biases	88	88	94
2) Gravity, drag, s.r.p coord and ref errors	"	88	88	98
3) Drag, s.r.p, coord and ref errors	"	21	19	31
Note: s.r.p. = solar radiation pressure				

### 5.3 Geographical orbit error distribution

The representation of the radial orbit error in a geographical reference frame was achieved by generating the time history of the radial orbit differences along with the satellite ground track and then computing the mean and the root mean square (rms) values of the radial orbit error along all tracks within each of the regional blocks that the global surface was divided into. Figures 3, 4 and 5 illustrate the geographical distribution of the radial orbit error in terms of a mean orbit error and a variability about the mean for each regional block with the effects of all error sources included. The mean orbit error has large negative values in most of the regional blocks between the longitude meridians  $0^\circ-60^\circ$  and  $240^\circ-300^\circ$  regardless of the tracking scenario. This characteristic is dependent on the gravity error model used in this analysis. The root mean square values of the radial orbit error is lower for Scenarios A and B than for Scenario C in almost all of the regional blocks. Thus a more uniform distribution of the tracking sites and the corresponding larger data set reduces

the variability of the radial orbit error over most geographical areas.

## 6. RELATED RESEARCH

Some selected TRANET-II tracking data has been made available for the Navy's Geodetic Satellite (GEOSAT). GEOSAT is only 50 km lower than NROSS, so experiments performed using actual TRANET data should be applicable to NROSS as well. One of the most obvious results from these experiments is that the TRANET tracking system is currently operating at about 3 to 4 mm/sec rather than the 1 mm/sec precision assumed in the NROSS simulations. The source of this noise level is being investigated.

To determine the effect of reducing the number of tracking stations, several cases were studied and these are summarized in Table 5. A 2-day arc was chosen out of the 6 days for which TRANET data was provided, and the entire tracking network was used to obtain a reference trajectory. No altimeter data was available for an independent orbit accuracy evaluation, but presumably this would be as close to the true orbit as could be obtained with these data. Subsets of the tracking stations were then used to obtain orbits which were compared to the reference trajectory. Using only the 19 permanent stations which tracked GEOSAT results in very small changes from the reference orbit, while using just the four- to five-station network leads to much larger differences regardless of the distribution of those stations.

## 7. SUMMARY

The simulated data studies indicate that the effects of the dynamic model errors, particularly gravity errors, dominate over the "long" arc in all three scenarios, while the measurement model errors had greater effect in the "short" arcs. The radial orbit accuracy can be improved by "tuning" the geopotential harmonic coefficients in a post-flight environment, but this procedure could be

TABLE 5  
 GEOSAT 7/10/85-7/12/85  
 2-DAY ARC ORBIT COMPARISON SUMMARY

Case	Passes	No. of Obs.	RMS of Orbit Fit (cm/sec)	Radial Diff. (m) Largest/RMS
44 stations	254	7677	0.628	
N. America 4 stations	27	821	0.438	1.11/0.45
Europe 5 stations	35	1044	0.466	1.17/0.56
Global 5 stations	25	696	0.605	1.19/0.51
19 permanent stations	129	3861	0.669	0.15/0.06
Estimating initial conditions, pass biases, troposphere parameter, drag and reflectivity. PGS-S4 gravity field, stations estimated from 6-day arc.				

executed successfully only in Scenarios A and B where the geographical distribution of the doppler tracking sites over the globe is more uniform. Otherwise, it is likely that severe geographically correlated errors will occur in the tuned gravity field [5].

The effects of measurement model errors including station coordinate errors and troposphere refraction errors could be mitigated by using a larger measurement data set over a longer arc length for the analysis. It was not possible to obtain a good orbit fit over the "short" arc with Scenario C owing to the sparseness of the data set. The 23-station tracking network in Scenario B performed as well as the 43-station network in Scenario A in spite of the fact that the data set in Scenario A had at least 2700 more observations than the data set in Scenario A. This result could probably be explained by the fact that in Scenario A, there were dense concentrations of tracking sites in certain geographical areas, which caused the orbit to be fit more closely over these areas and to flare out in other less densely tracked regions. Proper sampling or weighting the data would undoubtedly improve the 43-station results.

The analysis of the data from the current GEOSAT mission appears to be consistent with the simulation results. Very little difference was seen between the 44- and 19-station orbits, while meter-level differences occur when the tracking is reduced to the four-station level regardless of their distribution. However, if one estimates that the best orbits are accurate to 50-70 cm radial rms, then even the worst tracking scenarios are providing orbits with 1 to 1.5 m radial rms accuracy.

#### 8. CONCLUSIONS

The applicability of a particular tracking network would appear to depend strongly on the orbit accuracy requirements. One- to two-meter radial orbit accuracies are fairly easily obtained with current gravity models and almost any tracking scenario if the arcs are long enough. However, if more accurate orbits are required, either the arcs must be shortened to reduce dynamical model error effects, the gravity models must be improved significantly, or some postlaunch gravity "tuning" is necessary. The latter technique can be successfully employed only if the tracking is fairly global, or geographically correlated errors will occur in the resulting geopotential field. In this case, all of the permanent sites and possibly many of the portable sites may be required. The same is true if the arcs are merely shortened, since there must be enough well distributed data to average out measurement model errors. Thus only the denser tracking networks are likely to provide radial orbit accuracies significantly below the 1 meter level.

## REFERENCES

- [1] Born, G. H., Some consideration for N-ROSS mission design, Center for Space Research Memorandum, December 1983.
- [2] Lerch, F. J., S. M. Klosko, and G. B. Patel, A refined gravity model from LAGEOS (GEM-L2), *Geophys. Res. Lett.*, 9 (11), 1263-1266, November 1982.
- [3] Lerch, F. J., B. H. Putney, C. A. Wagner, and S. M. Klosko, Goddard earth models for oceanographic applications (GEM10B and 10C), *Mar. Geod.*, 5 (2), 1981.
- [4] Shum, C. K., J. C. Ries, B. D. Tapley, P. Escudier, and E. Delaye, Atmospheric drag model for precision orbit determination, *CSR-86-2*, Center for Space Research, The University of Texas at Austin, January 1986.
- [5] Rosborough, G. W., Satellite orbit perturbations due to the geopotential, *CSR-86-1*, Center for Space Research, The University of Texas at Austin, January 1986.

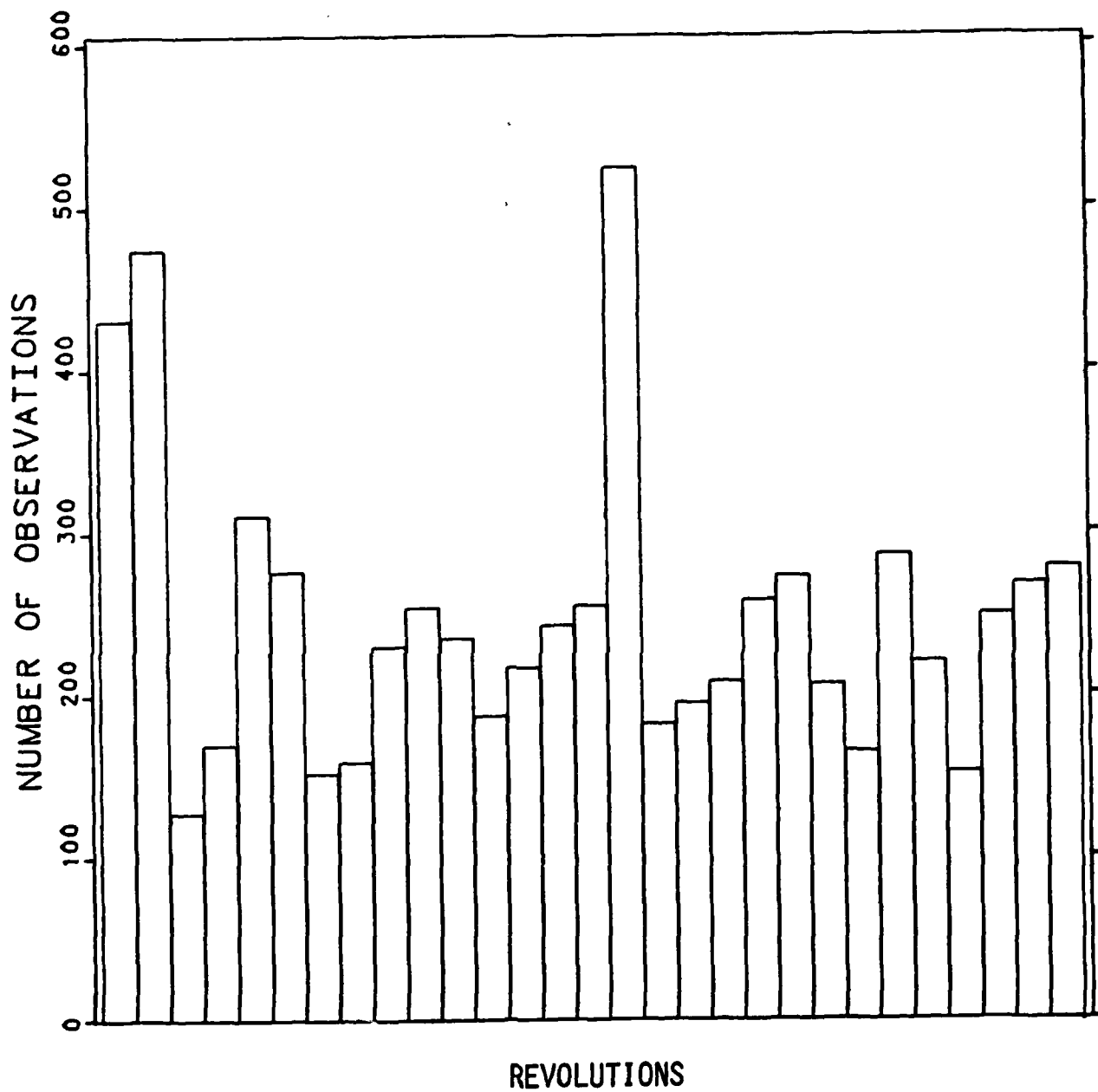


Figure 1. Histogram of simulated doppler tracking for NROSS 2-day arc .

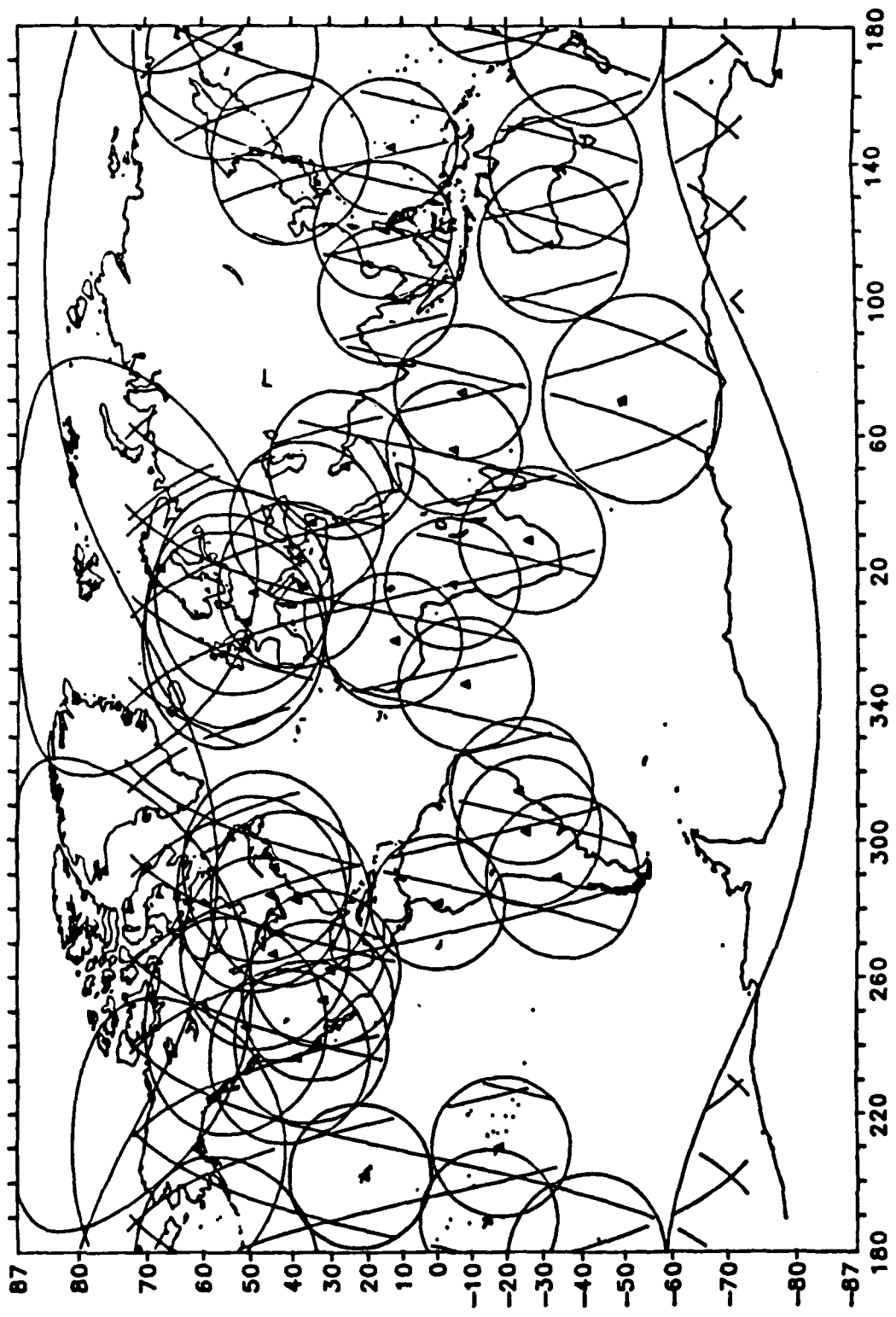


Figure 2. Groundtrack simulated doppler tracking for NROSS 2-day arc .

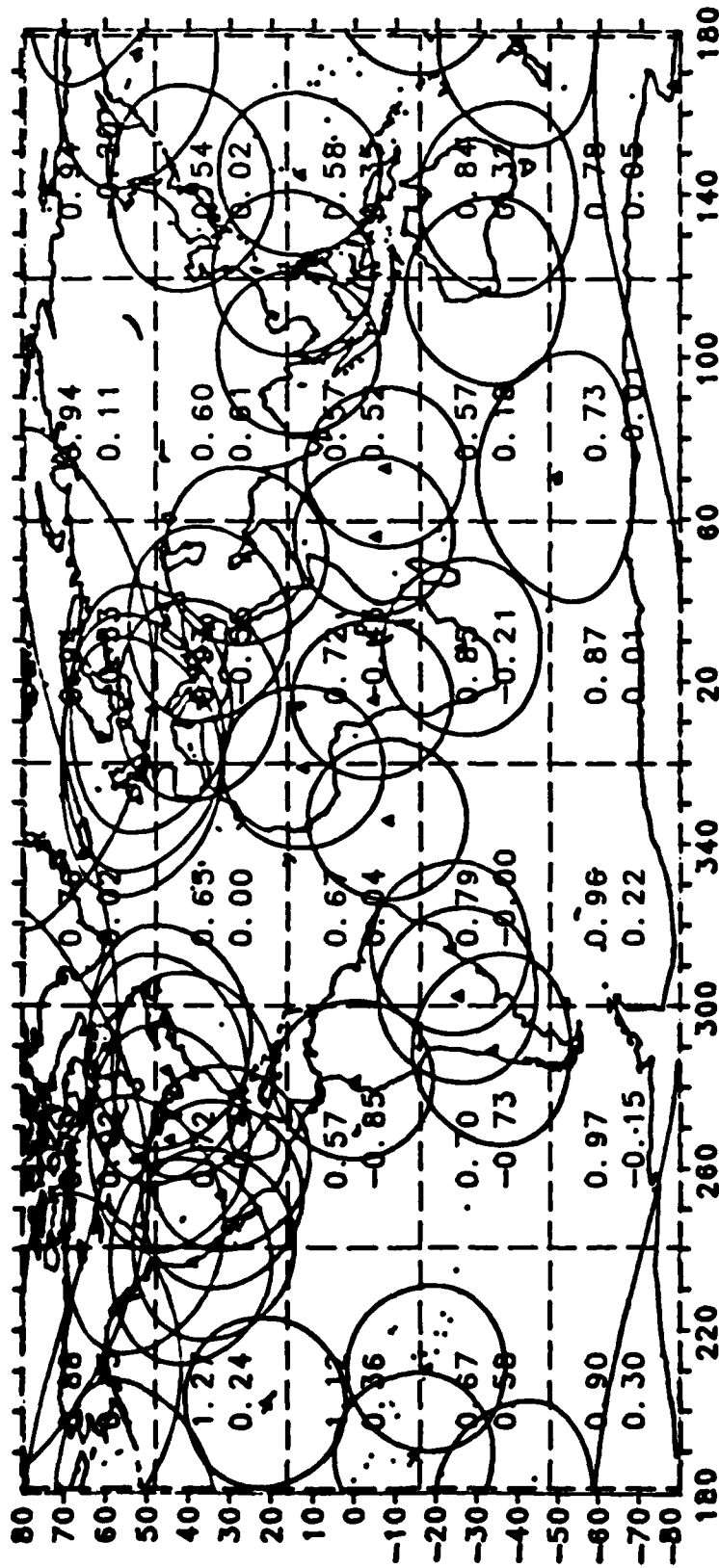


Figure 3. Radial orbit error for NROSS 2-day arc (rms/mean). Gravity, drag, solar radiation pressure, station coordinate and refraction errors (43 stations).

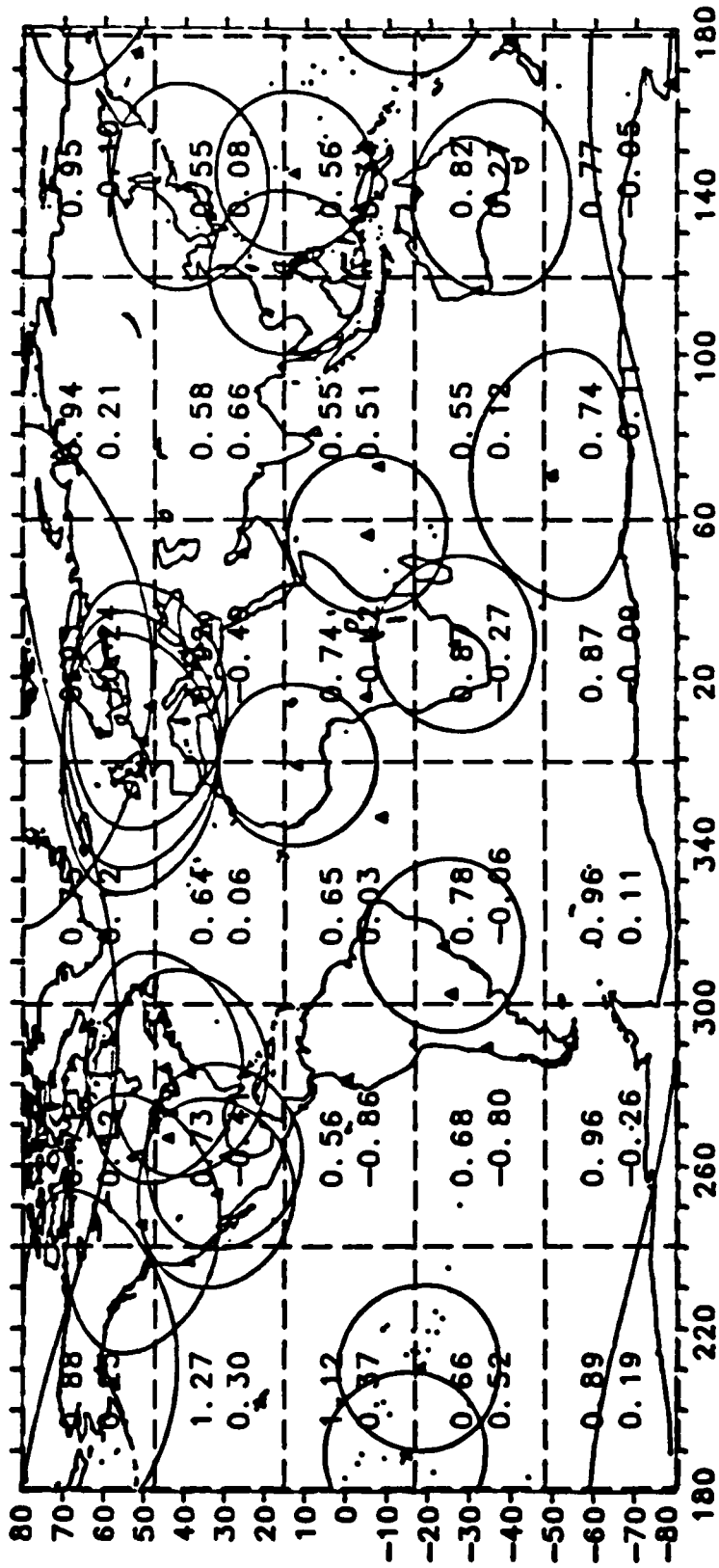


Figure 4. Radial orbit error for NROSS 2-day arc (rms/mean). Gravity, drag, solar radiation pressure, station coordinate and refraction errors (23 stations).

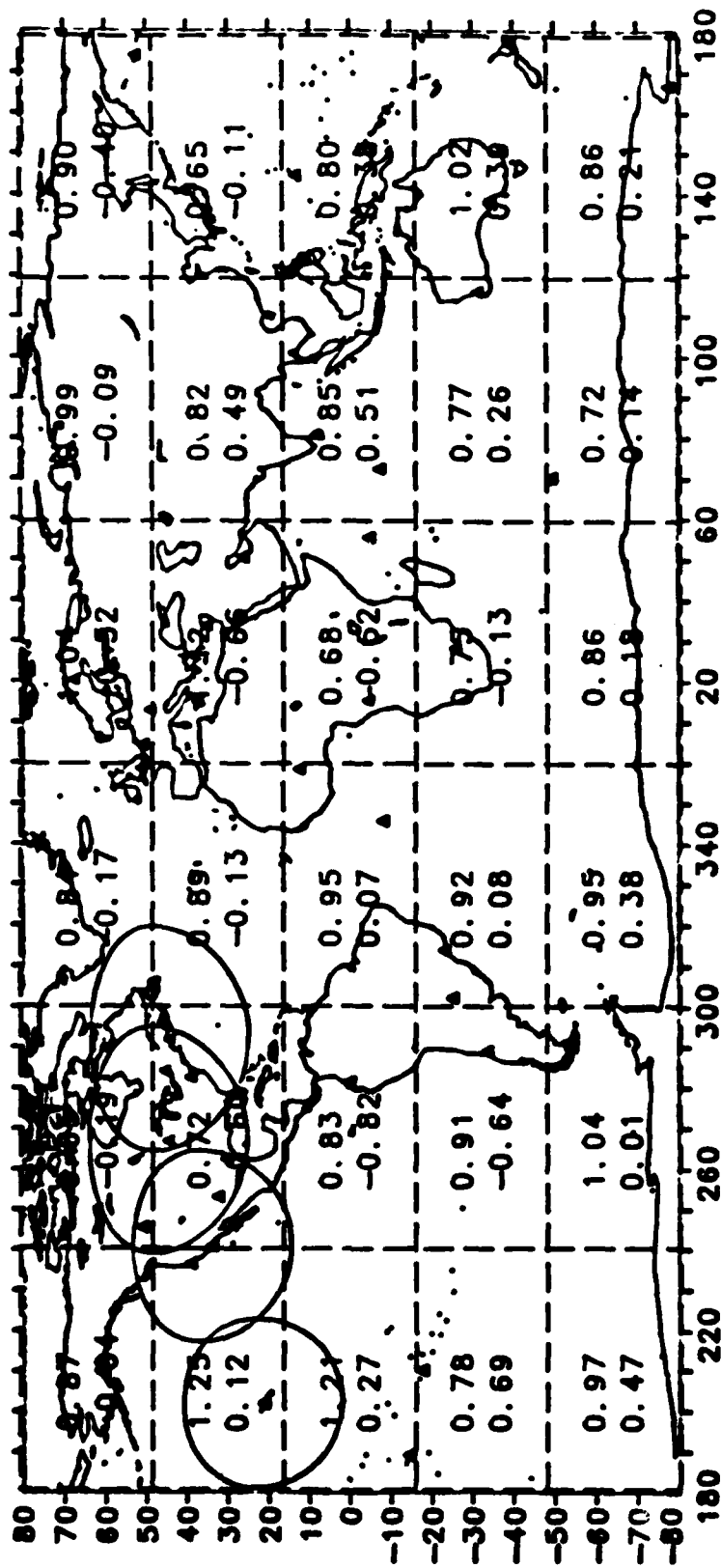


Figure 5. Radial orbit error for NROSS 2-day arc (rms/mean). Gravity, drag, solar radiation pressure, station coordinate and refraction errors (4 stations).

ENM

11-80

DTIC